CHAPTER IV

THERMOCAPILLARY MIGRATION OF A BUBBLE CLOUD

4.1 Introduction

In many engineering applications, where thermocapillary motion of bubbles and drops is important, it is likely that many bubbles or drops are present. In most cases, we may also expect bubbles or drops of different size. It is therefore important to understand the overall behavior of large bubble systems, with either mono-disperse or polydisperse bubbles. In this chapter, we first present simulations of equal-sized bubbles in both two and three dimensions. Then, similar simulations are conducted for non-equal-sized bubbles in both two- and three-dimensions.

4.2 Mono-dispersed systems

To investigate the interaction of many bubbles, we first compute the evolution of six bubbles. The resolution is the same as in the two bubbles case discussed in Section 3.5, i.e., 128×256 grid points for a $x/a = 10$ and $y/a = 20$ computational box. The initial positions are selected arbitrarily. The non-dimensional numbers for this case are $Re = 5, Ma = 20, Ca = 0.01666$ while the ratio of the physical properties is 0.5.

Figure 4.1 and Figure 4.2 show the velocity field and the isotherms in the laboratory frame, respectively, at different times. We see from the plots that two bubbles separate from the rest and rise ahead, while the others start lining up across the channel. Later on, the two leading bubbles move side by side and rise almost independent of the other bubbles. Their motion is similar to the two-bubble interaction in Figure 3.24. Figure 4.3 shows a more quantitative description of this simulation where the migration velocity, the vertical positions, the internal circulation and the deformation are plotted. Examining the velocity of each bubble in Figure 4.3(a) and (b), we see that the velocity of the center of mass of the bubble cloud reaches a steady state, while each individual bubble does not. In particular, each bubble in the group of four, has oscillating rise velocities. Also, the leading bubbles rise faster than the four bubbles left behind. Since the leading two bubbles move apart horizontally, their deformation is small at steady state compared with the other ones which are squeezed across the channel. This is clear in Figure 4.3(d). The trajectories of each bubble is shown in Figure 4.4, which clearly shows the separation of the two leading bubbles from the other bubbles. The average temperature distribution at the time of the last frame is plotted in Figure 4.5(a) where the initial temperature distribution is shown by the straight line. The average temperature fluctuations are plotted in Figure 4.5(b). As the bubbles rise, they perturb the initial linear temperature profile. The bubbles carry cold fluid with them upward and a warmer fluid flows back between them to conserve mass. Since the thermal capacity of the bubbles is less than of the outer fluid, the net effect is to heat the region around and behind the bubbles. This is clear in Figure 4.5. The temperature increases above the linear temperature profile where the two top bubbles are and even more across the bottom four bubbles. Since the temperature of the bottom wall is fixed, the gradient in the

bottom region must increase, as is also seen in the close spacing of the isotherms in Figure 4.2.

We have computed similar interactions for four bubbles and found that for two different initial conditions they line up across the channel as they move towards the hot wall. Oscillations in their rise velocities were similar to the six bubble case.

To investigate whether the layer formation suggested by the simulations shown above is a prominent feature in large bubble clouds, we have conducted simulations on a larger systems where we place sixteen equal sized bubbles in a domain which is 11.43 bubble radius large in both directions. The resolution is 256×256 grid points and the non-dimensional numbers are the same as in the six bubble simulation. Figure 4.6 shows the velocity field at different times while the isotherms are plotted in Figure 4.7. The bubbles form two layers, as seen in the first three frames. Since the sides of the box are not occupied by any bubbles, the hot ambient fluid flows down in this region. Bubbles are close to each other in the top layer and this decreases the down flow of ambient fluid. As a result of this behavior, the bubbles in the top layer move toward the sides of the box. As the top layer moves, the whole picture is nearly symmetric with respect to the middle vertical line. The first layer opens up like an envelope. The bubbles in that layer carry the cold fluid with them, forming a cold region between the two layers. After the sixth frame, the top layer breaks up, allowing the hot ambient fluid to flow down between the bubbles. This is clear from both the velocities and the isotherms. Similarly, at this time, the lower layer also breaks up into two horizontal layers due to the temperature gradient in the cold region between the two layers. After the break up, the hot ambient fluid flows down quickly in the middle of the box. This causes the fluid to heat up in that region, changing the temperature gradient. By moving in the direction of the temperature

bottom region must increase, as is also seen in the close spacing of the isotherms in Figure 4.2.

We have computed similar interactions for four bubbles and found that for two different initial conditions they line up across the channel as they move towards the hot wall. Oscillations in their rise velocities were similar to the six bubble case.

To investigate whether the layer formation suggested by the simulations shown above is a prominent feature in large bubble clouds, we have conducted simulations on a larger systems where we place sixteen equal sized bubbles in a domain which is 11.43 bubble radius large in both directions. The resolution is 256×256 grid points and the non-dimensional numbers are the same as in the six bubble simulation. Figure 4.6 shows the velocity field at different times while the isotherms are plotted in Figure 4.7. The bubbles form two layers, as seen in the first three frames. Since the sides of the box are not occupied by any bubbles, the hot ambient fluid flows down in this region. Bubbles are close to each other in the top layer and this decreases the down flow of ambient fluid. As a result of this behavior, the bubbles in the top layer move toward the sides of the box. As the top layer moves, the whole picture is nearly symmetric with respect to the middle vertical line. The first layer opens up like an envelope. The bubbles in that layer carry the cold fluid with them, forming a cold region between the two layers. After the sixth frame, the top layer breaks up, allowing the hot ambient fluid to flow down between the bubbles. This is clear from both the velocities and the isotherms. Similarly, at this time, the lower layer also breaks up into two horizontal layers due to the temperature gradient in the cold region between the two layers. After the break up, the hot ambient fluid flows down quickly in the middle of the box. This causes the fluid to heat up in that region, changing the temperature gradient. By moving in the direction of the temperature

gradient, the bubbles change direction toward the vertical middle symmetry line. The leading bubbles form a horizontal layer before hitting the wall. The bubbles in the lower layer form another layer by coming closer together horizontally due to the temperature gradient. This simulation suggests that while layers may form, they will break up through instability waves many times longer than the bubble diameter, but eventually they strive to form stable layers again. Figure 4.8 shows the migration velocity and the vertical position of each bubble. The trajectories of each bubble are plotted in Figure 4.9. Both of these figures demonstrate the formation of bubble layers.

After doing two dimensional simulations of bubble clouds, we move on to fully three dimensional simulations. The size of these computations is limited by the available memory and speed. Therefore, we conduct the three dimensional simulations with a resolution of $64 \times 64 \times 128$ grid points in a domain which extends 6.66 bubble radii in x and y directions and twice as large in the z direction. The non-dimensional numbers are the same as the two dimensional simulations for six and sixteen bubbles. To begin the calculations we place nine equal-sized bubbles, arbitrarily, but initialy close to the lower cold wall.

We show the migration of these bubbles toward the top hot wall at different times in Figure 4.10. Since the visualizations of the velocity field and the isotherms are not as easy as in two-dimensions, we show both quantities over the middle cross sectional plane, separately. The velocity field in the middle $x - z$ plane is plotted in Figure 4.11 and Figure 4.12 shows the velocity field in the middle $y - z$ plane. Similarly, the isotherms are plotted in the middle $x - z$ plane in Figure 4.13 while Figure 4.14 shows them in the $y - z$ plane. It is seen from both the velocity field and the isotherms in the $x - z$ plane that three bubbles form a layer by coming

side by side while migrating toward the upper wall. Since we are looking at a cross sectional plane, we only see a portion of this layer formation, which actually involves more than three bubbles. The wake of the bubbles perturbs the temperature field only slightly. The isotherms wrap around the bubbles showing the level of convective transport of energy. The middle $y-z$ cross sectional plane shows more information about the evolution. In Figure 4.12, three bubbles are present. Initially, they are close to each other. As they move up, one of the bubbles separates and moves faster than the other two bubbles which migrate almost side by side. The recirculation zone in the wake of the lower bubble is easily visible. This recirculation zone causes temperature disturbances all the way down to the lower wall. This effect is seen in Figure 4.14. The overall behavior of the nine bubbles is much clearer in Figure 4.10, Figure 4.15 and Figure 4.16. Figure 4.10 shows that one of the nine bubbles separates from the other bubbles and the others form a layer similar to what was seen in the two dimensional simulations. The number of bubbles is just enough to form one horizontal layer. The migration velocity and the vertical position also show this. One of the bubbles, which was originally ahead of others, separates easily from others. Figure 4.16 shows the trajectories from two different directions. The same behavior is seen here as well. These fully three dimensional simulations confirm the formation of bubble layers observed earlier in this section for the two dimensional simulations.

4.3 Polydispersed systems

Bubbles and drops of exactly the same size are unlikely to be present in real systems. In this section, we explore the interaction between different sized bubbles by both two and three-dimensional simulations.

We first examine the interaction among six bubbles. Three of the six bubbles are small and the other three are larger. The ratio of the small bubble radius to the large bubble radius is $\lambda = 3/5$. We define an average bubble radius, a_v, by calculating the arithmetic average of the radius of the bubbles. The average reference velocity, U_{rv}, is defined based on this average bubble radius. The non-dimensional numbers for the big bubbles are the same as for the six-bubble mono-dispersed case where $Re = 5$, $Ma = 20$, $Ca = 0.01666$ while the ratio of the physical properties is 0.5. The resolution is 128×256 grid points in a $x/a_v = 10$, $y/a_v = 20$ computational box.

We show the velocity field and the isotherms from this simulation at different times in Figure 4.17 and Figure 4.18, respectively. We see that the bubbles come together, forming a horizontal layer at early times. This is seen in frame one to four in both plots. Since the migration velocity is proportional to the bubble radius, it should be expected that small bubbles move with a lower velocity than big ones. This, however, is only true when the bubbles are isolated. As seen in both figures, the small bubbles move very close to the big ones and almost "stick" to the sides of the big bubbles. This is particularly clear in the second half of the evolution. As we follow the interaction in the second half, it is seen that two big bubbles collide with the third big one which is ahead of others. This causes the third bubble to separate from the other bubbles and reach the upper wall, well ahead of others. Although the small bubbles migrate to the side of the big ones, they form a horizontal layer across the channel. This is clearly seen in Figure 4.17 and Figure 4.18 for the second half of the evolution. The reason that the small bubbles also migrate as fast as the big bubbles is due to the fact that the small bubbles are caught in the wake of the large bubbles. Due to this behavior, the thermal gradient across the small bubbles are higher and hence,

their velocity is large as well. In Figure 4.19, we show a quantitative description of this simulation where the migration velocity, the vertical position, the internal circulation and the deformation of each bubble are plotted. We plot the trajectories of each bubble as well as that of the center of mass of the cloud in Figure 4.20. The formation of the bubble layer is seen from the migration velocity and the vertical position as well as from the trajectories. When the leading bubble collides with the upper wall, it deforms considerably. Since this bubble migrates independently from the rest, in the second half of the simulation, its internal circulation should diminish. This is indeed the case as seen in Figure 4.19(c). The results here are similar to the six-bubble mono-dispersed case in that once bubbles fill the channel horizontally, the other bubbles form a second layer.

As for the mono-disperse case, we have simulated larger system of non-equal-sized bubbles. We place sixteen bubbles in a domain which extends 13.33 average bubble radii in both directions. We select the number of small and big bubbles equally, namely eight big and eight small bubbles. The resolution is 256×256 grid points for this case. The ratio of small bubble radius to large bubble radius is $\lambda = 5/7$. All other non-dimensional numbers for the big bubbles are the same as for the previous sixteen-bubble mono-dispersed case.

We follow the interaction of these bubbles in Figure 4.21 where both the bubbles and the velocity field are shown at different times. The corresponding isotherms are plotted in Figure 4.22. The figures show behavior similar to Figure 4.6 and Figure 4.7. In the top frames, by accelerating very quickly, the bubbles changes their initial configuration and move close to each other. Since the sides of the box are not occupied by any bubbles, initially, the hot ambient fluid flows down there, rather than between the bubbles. This results in the thermal gradient seen in Figure 4.22.

Due to this thermal gradient, some of the leading bubbles move toward the sides of the domain. As these bubbles separate from the others, the rest of the bubbles form a layer, as seen in the middle frames of the same plot. Because of different bubbles sizes the layer is not as uniform as for the mono-dispersed case. Nevertheless, this layer across the channel persists until the end of the simulation. The leading bubbles slow down when they get close to the upper wall and, since the others move faster, eventually all the leading bubbles come to the same horizontal level before hitting the top wall. The lower layer continue to migrate during this period. The migration velocity and the vertical position of each bubble, in Figure 4.23, as well as the trajectories of the bubbles, in Figure 4.24, also show this behavior. The separation of the leading bubbles and the formation of the bubble layer is clear in those plots. The formation of bubble layers, until the channel is filled horizontally, is quiet similar to the mono-dispersed case that was analyzed earlier.

Finally, in order to further verify bubble layer formation for real polydispersed systems, we have conducted a fully three dimensional simulation of unequal-sized bubbles. The resolution in this simulation is $64 \times 64 \times 128$ grid points. The ratio of bubble radii is $\lambda = 2/3$. We place nine bubbles arbitrarily, close to the lower wall. Five out of the nine bubbles are small. The non-dimensional numbers for big bubbles are the same as in the previous cases. The size of the computational box is $x/a_v = 8$, $y/a_v = 8$, and $z/a_v = 16$. The average bubble radius and the average reference velocity are used to scale the quantities computed in this simulation.

The migration of these bubbles toward the top hot wall at different times is shown in Figure 4.25. To show the structure of the velocity field and the isotherms in this simulation, we have chosen the middle cross sectional planes to plot them (similar to the nine-bubble mono-dispersed case). Figure 4.26 and Figure 4.27 show the velocity

field in the $x-z$ and $y-z$ planes, respectively. By examining the migration of the bubbles in Figure 4.25, it is observed that the large bubbles eventually overtake the small bubbles and move ahead of them. This is also seen from the velocity field in Figure 4.26 and in Figure 4.27. Since the migration velocity is proportional to the bubble radius, the larger bubbles migrate faster than the smaller bubbles and it is not surprising that the larger bubbles overtake the rest. This is also seen in the isotherms, which are plotted in Figure 4.28 and Figure 4.29, for the same middle planes. Inspection of the isotherms shows that convective transport of energy is considerable and leads to curved isotherms inside the bubbles as well as in the wake of the bubbles. This wrapping of the isotherms around the bubbles reduces the migration velocity of each bubble because of the more uniform temperature distribution along the bubble surface. In Figure 4.30, we show the migration velocity and the vertical position of each bubble. The trajectories are shown Figure 4.31 from two different directions. In these figures, the bubbles marked by 2, 4, 6, and 8 correspond to the big bubbles. The migration velocity of each bubble in Figure 4.30(a) clearly indicates that the larger bubbles have higher velocities and their migration velocities are similar. The smaller bubbles also have migration velocities close to each other, but each group has a different velocity. Of course, the consequence of this is the two layer formation shown in Figure 4.30(b) as well as in Figure 4.31. This result confirms that the bubble layer formation seen in two dimensional simulations, is also a prominent feature in real polydisperse bubbly flows. But, in contrast to the two dimensional simulations of polydispersed system, where the bubbles of different size form a horizontal layer by migrating close to each other, it is found in three dimensional simulation of a polydisperse system that different types of bubbles form different layers. Each layer moves with a different velocity and the larger the bubbles, the higher the migration

velocity of each layer. This results in a feature that the layer of large bubbles move as a top layer and the small bubbles move behind as a lower layer. This is a distinct behavior of three dimensional simulations of polydispersed systems.

4.4 Conclusion

In this chapter, we have examined the behavior of a bubble cloud in thermo-capillary flows in zero gravity for both mono-disperse and polydisperse cases. The numerical simulations of mono-disperse systems show that the bubbles form horizontal layers. As soon as the bubbles form one layer that fills the channel horizontally, the rest of the bubbles form another layer. Although we saw, in the two dimensional sixteen bubbles simulation, that this may layer break up by instability waves, the layer is eventually regenerated. Three dimensional simulations confirm this formation of bubble layers and simulations of bubbles in polydisperse systems show the same behavior. In contrast to two dimensional simulations of polydispersed system, where bubbles of different size form a horizontal layer, the three dimensional simulation of a polydispersed system shows that different sizes of bubbles form different layers. Each layer moves with a different velocity and the larger the bubbles, the higher the migration velocity of each layer. This results in a layer of large bubbles that moves ahead of a layer of small bubbles. While the prominent feature of layer formation is a persistent characteristic in these simulations, only bubbly flows are explored here. In the light of Chapter III, where two dimensional drops were examined, we do not expect drops to form layers at high Re and Ma.

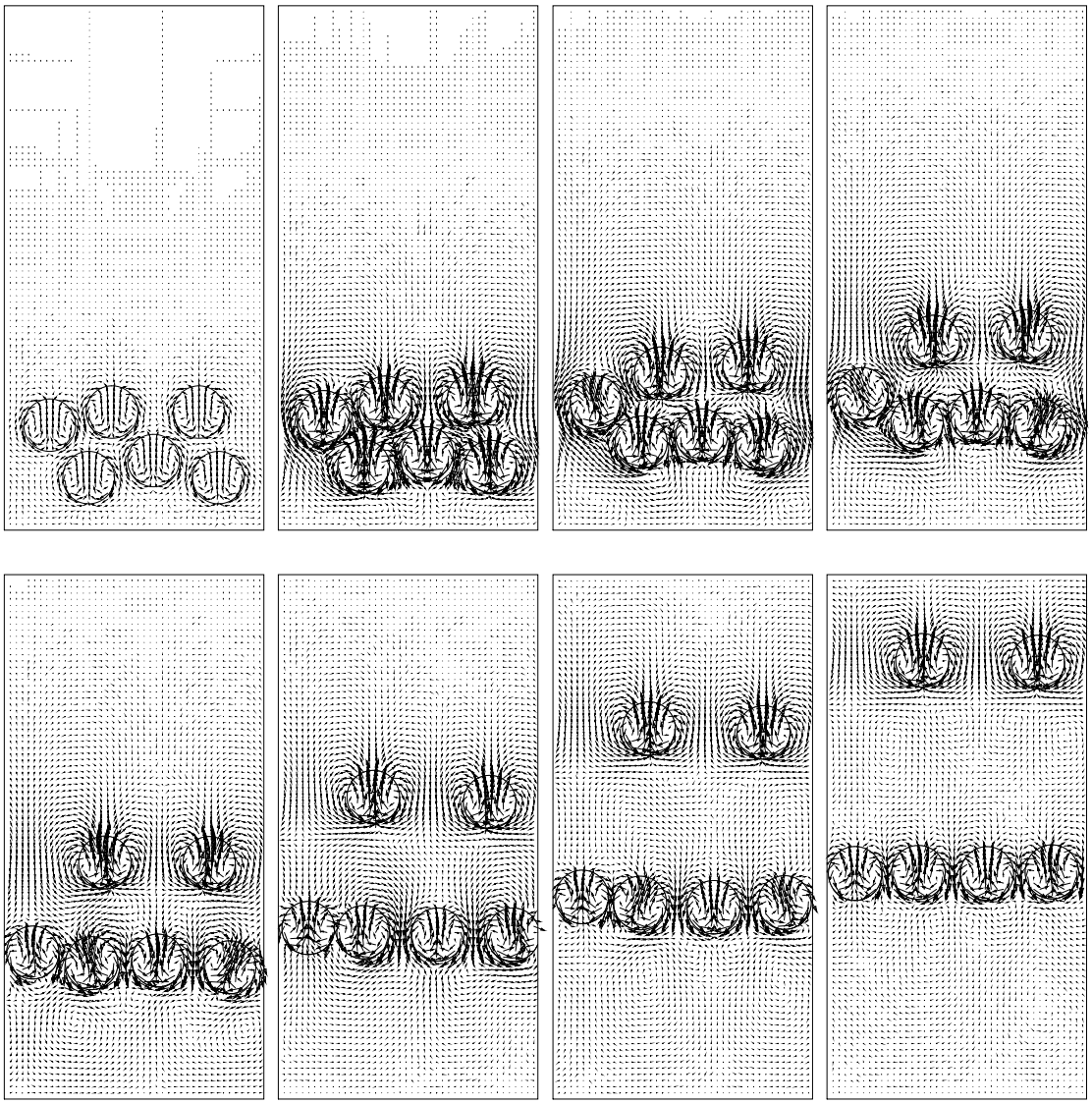

Figure 4.1: Velocity field for selected frames from the computation of six bubble interaction. The velocity field is shown at every third grid point. Time progresses from left to right. The nondimensional time, t^*, is equal to $0.25, 5, 15, 25, 40, 62.5, 87.5, 112.5$. The nondimensional time is scaled by a/U_r and velocity is scaled by reference velocity, U_r. Computational domain size is $x/a = 10$ and $z/a = 20$. Here, $Re = 5$, $Ma = 20$ and $Ca = 0.01666$.

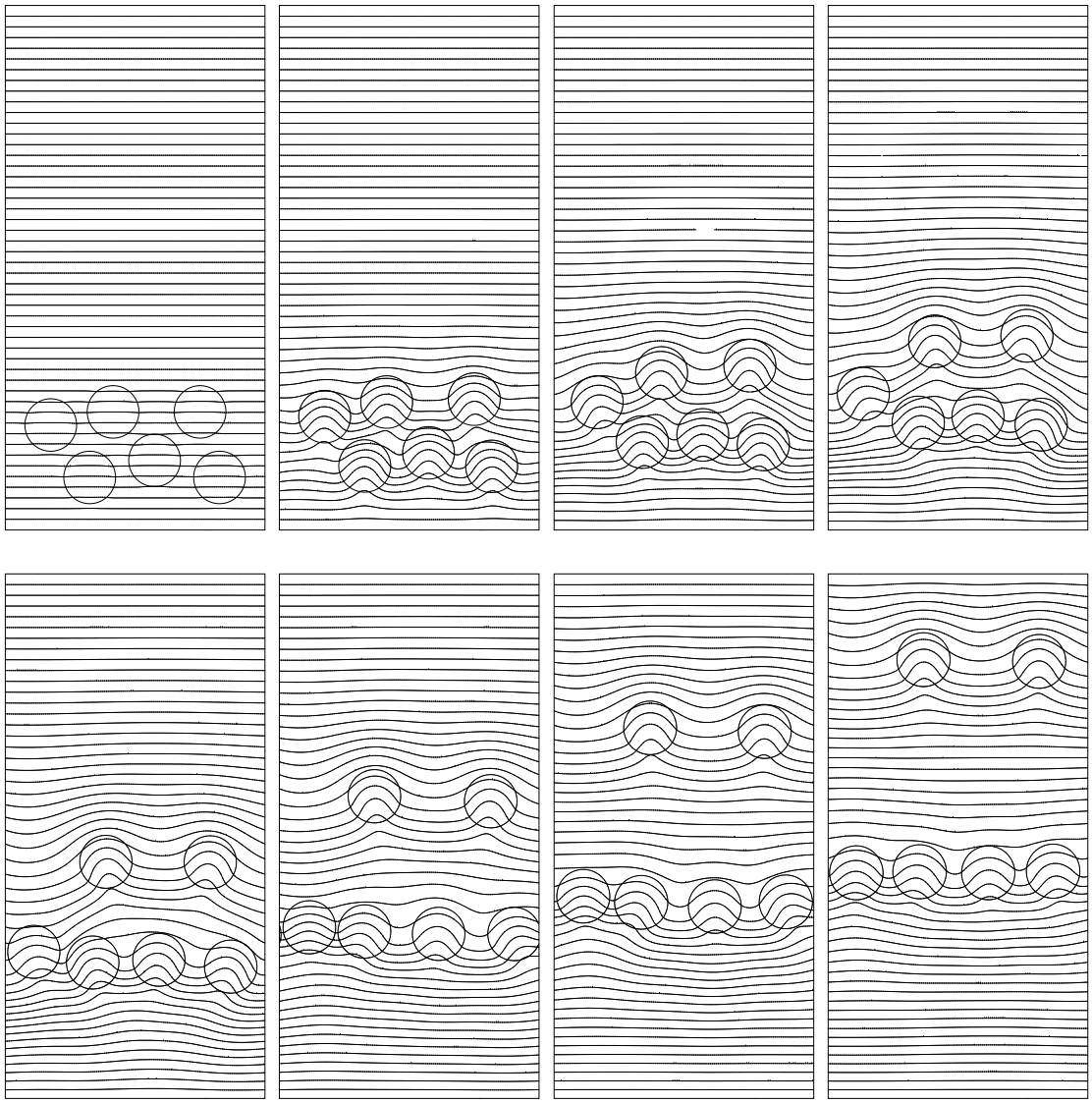

Figure 4.2: Temperature contours for selected frames from the computation of six bubble interaction in Figure 4.2. 50 equally spaced contours are shown. Time progresses from left to right. The nondimensional time, t^*, is equal to $0.25, 5, 15, 25, 40, 62.5, 87.5, 112.5$. The nondimensional time is scaled by a/U_r and temperature is scaled, after subtracting a reference temperature, by $a\nabla T_\infty$. Computational domain size is $x/a = 10$ and $z/a = 20$.

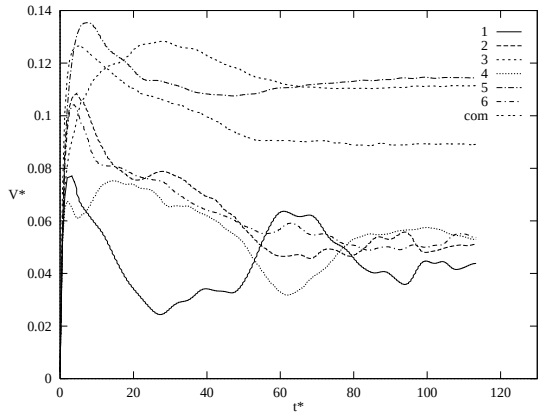

(a) Migration velocity

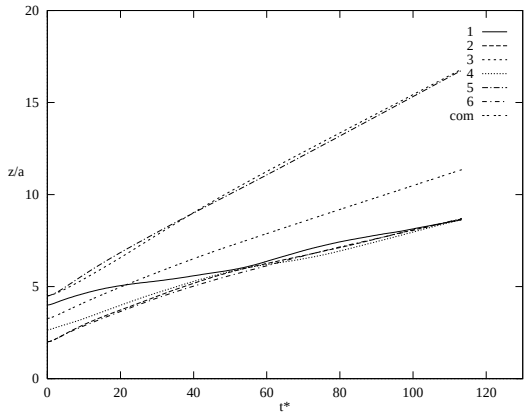

(b) z component of the centroid of bubbles

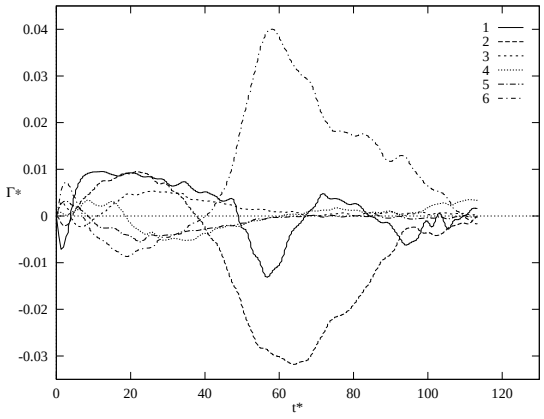

(c) Internal circulation

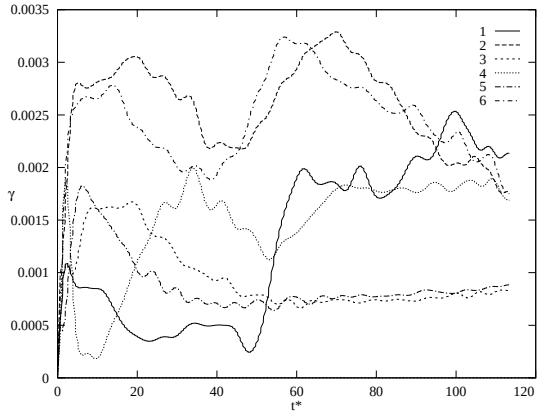

(d) Deformation

Figure 4.3: Quantitative description of the six bubble interaction in Figures 4.2 and 4.3. (a) Migration velocity versus time. (b) z component of the centroid of bubbles versus time. (c) Internal circulation versus time. (d) Deformation versus time. Velocity is scaled by U_r, z axis by a, time by a/U_r, and the internal circulation by $2\pi a U_r$. Bubbles marked 1 to 6 from left to right in the domain. Com is the velocity of the center of mass.

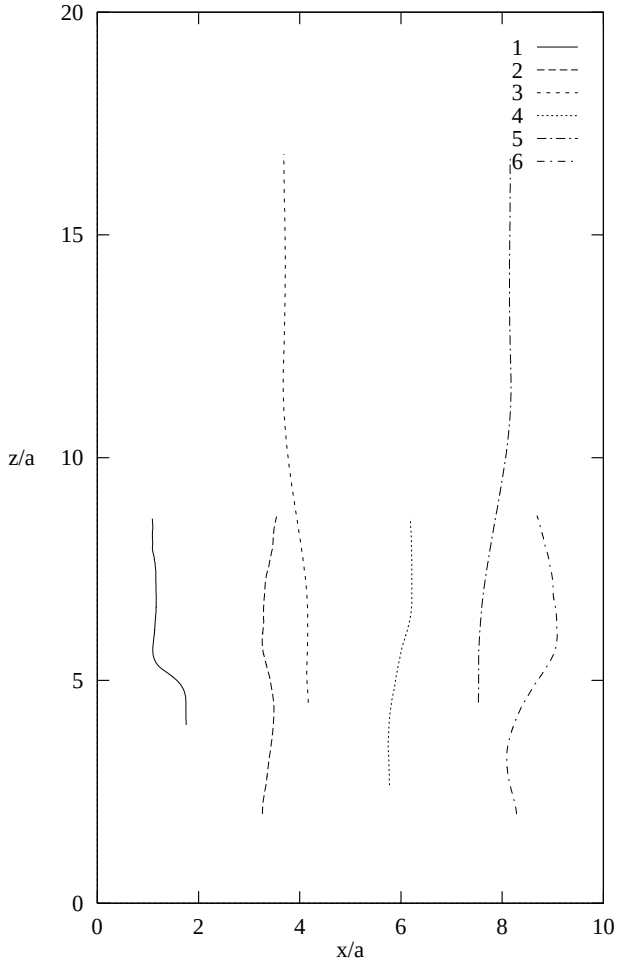

Figure 4.4: Trajectories of the center of mass of the bubbles. Both axis are scaled by the bubble radius a.

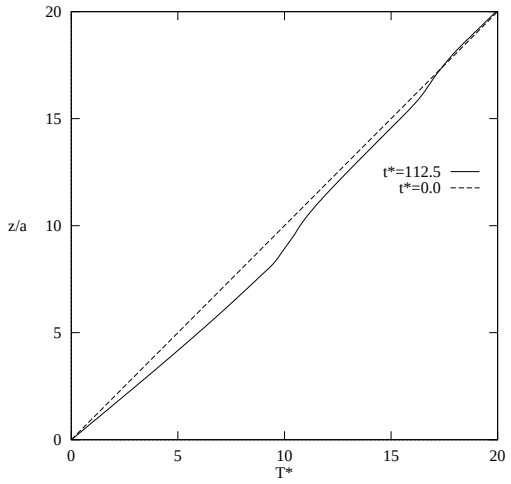

(a) The average temperature

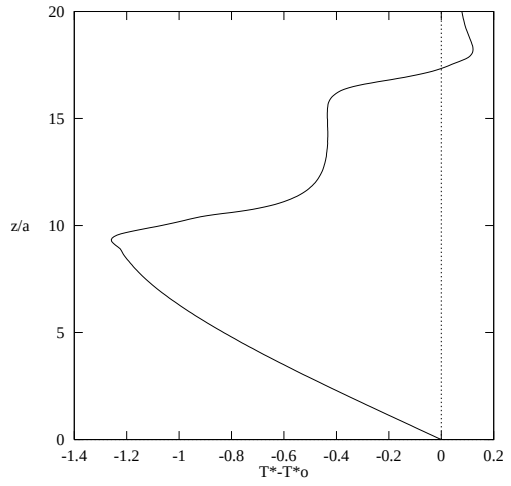

(b) The average temperature fluctuation

Figure 4.5: (a) The average temperature (b) The average temperature fluctuation, versus vertical direction at $t^* = 112.5$. Note that the initial temperature distribution at $t^* = 0.0$ is shown by straight line. Temperature is scaled, after subtracting a reference temperature, by $a\nabla T_\infty$.

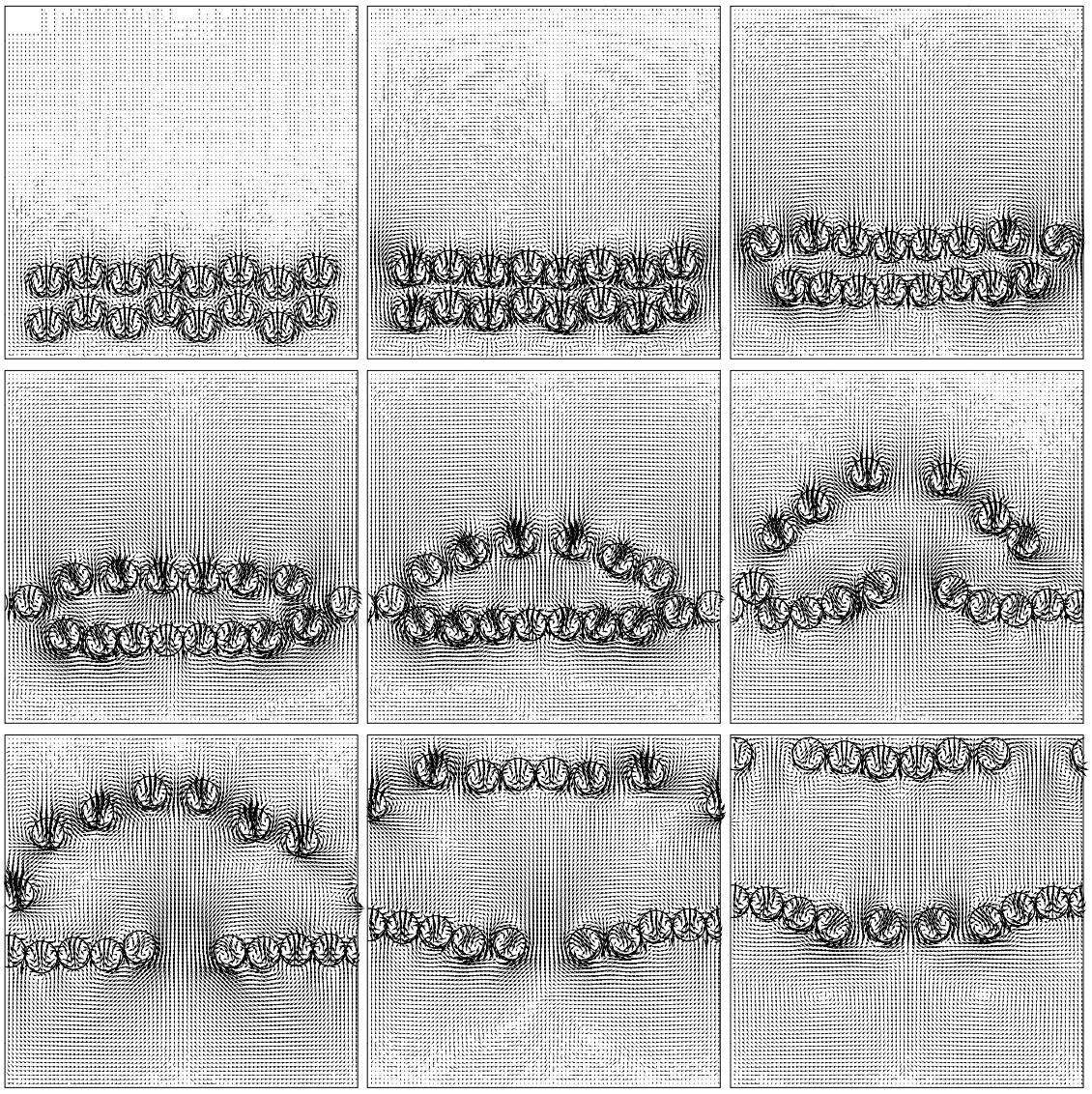

Figure 4.6: Velocity field for selected frames from the simulation of 16 bubble interaction. The velocity field is shown at every third grid point. Time progresses from left to right, top to bottom. The nondimensional time, t^*, is equal to 1.4, 14.3, 64.3, 107, 142.85, 214.3, 285.7, 357.14, 428.6. The nondimensional time is scaled by a/U_r and velocity by U_r. Computational domain size is $x/a = 11.43$ and $z/a = 11.43$. Here, $Re = 5$, $Ma = 40$ and $Ca = 0.01666$.

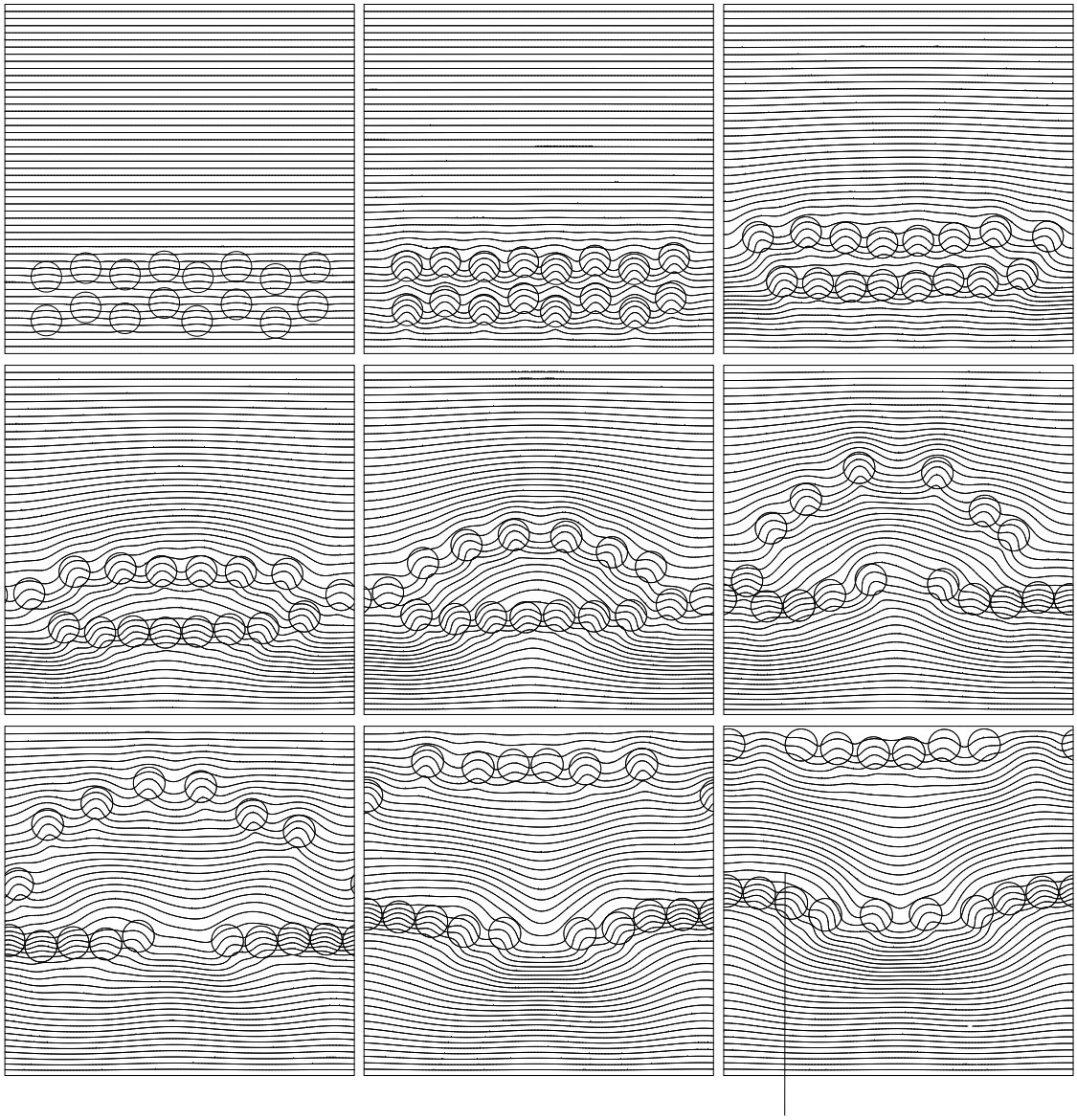

Figure 4.7: Temperature contours for selected frames from the simulation of 16 bubble interaction in Figure 4.6. 50 equally spaced contours are shown. Time progresses from left to right, top to bottom. The nondimensional time, t^*, is equal to 1.4, 14.3, 64.3, 107, 142.85, 214.3, 285.7, 357.14, 428.6. The nondimensional time is scaled by a/U_r and temperature is scaled, after subtracting a reference temperature, by $a\nabla T_\infty$. Computational domain size is $x/a = 11.43$ and $z/a = 11.43$.

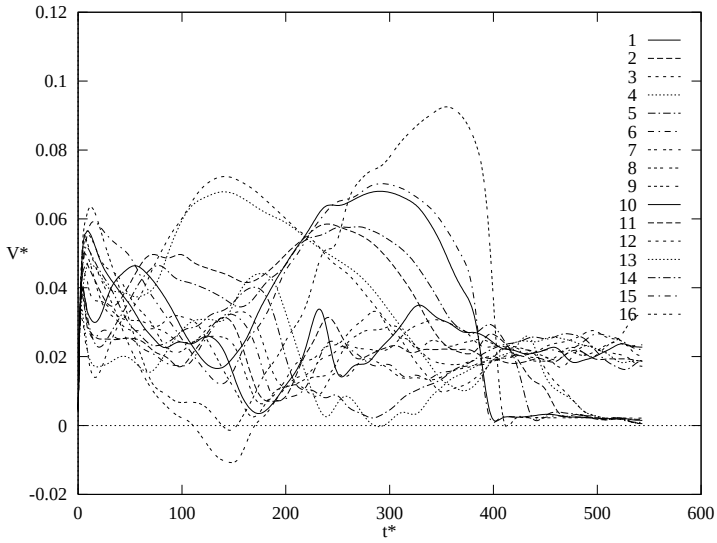

(a) Migration velocity

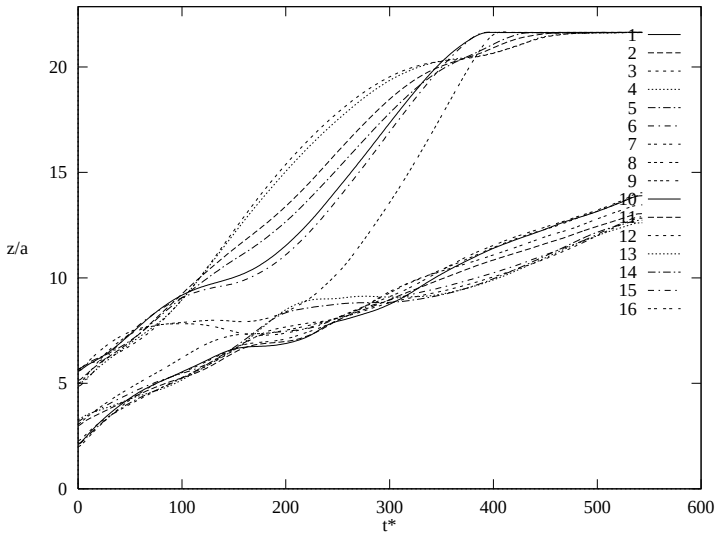

(b) z component of the centroid of bubbles

Figure 4.8: (a) Migration velocity versus time (b) z component of the centroid of bubbles versus time for 16 equal-sized bubble interaction in Figures 4.6 and 4.7. Velocity is scaled by reference velocity U_r, time is scaled by a/U_r and z axis by a.

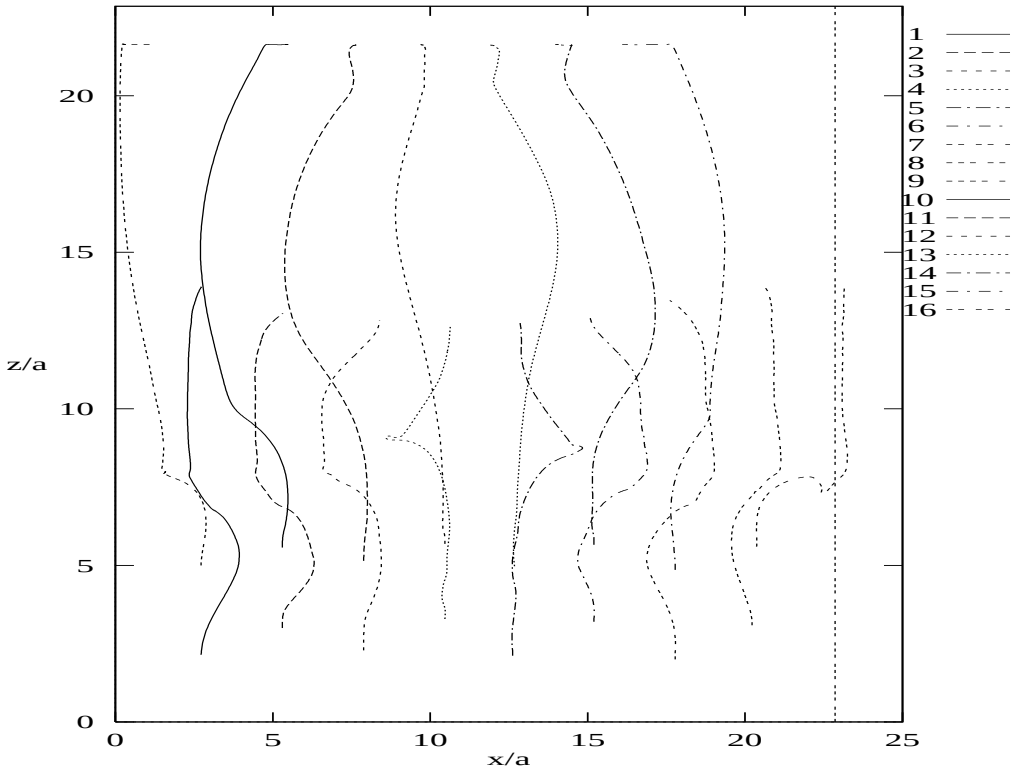

Figure 4.9: Trajectories of the center of mass of the bubbles. Both axis are scaled by the bubble radius a.